Animal 18 (2024) 101129

Contents lists available at ScienceDirect

Animal
The international journal of animal biosciences

Genome-wide association study of growth curve parameters reveals novel genomic regions and candidate genes associated with metatarsal bone traits in chickens

S.Z. Wang [a,b,c,1], M.D. Wang [a,b,c,1], J.Y. Wang [a,b,c], M. Yuan [a,b,c], Y.D. Li [a,b,c], P.T. Luo [d], F. Xiao [d], H. Li [a,b,c,*]

[a] Key Laboratory of Chicken Genetics and Breeding, Ministry of Agriculture and Rural Affairs, Harbin 150030, PR China
[b] Key Laboratory of Animal Genetics, Breeding and Reproduction, Education Department of Heilongjiang Province, Harbin 150030, PR China
[c] College of Animal Science and Technology, Northeast Agricultural University, Harbin 150030, PR China
[d] Fujian Sunnzer Biotechnology Development Co. Ltd, Guangze, Fujian Province 354100, PR China

ARTICLE INFO

Article history:
Received 26 October 2023
Revised 2 March 2024
Accepted 5 March 2024
Available online 12 March 2024

Keywords:
Genetic basis
Growth and development
Non-linear models
Quantitative trait loci
Skeleton

ABSTRACT

The growth and development of chicken bones have an enormous impact on the health and production performance of chickens. However, the development pattern and genetic regulation of the chicken skeleton are poorly understood. This study aimed to evaluate metatarsal bone growth and development patterns in chickens via non-linear models, and to identify the genetic determinants of metatarsal bone traits using a genome-wide association study (**GWAS**) based on growth curve parameters. Data on metatarsal length (**MeL**) and metatarsal circumference (**MeC**) were obtained from 471 F_2 chickens (generated by crossing broiler sires, derived from a line selected for high abdominal fat, with Baier layer dams) at 4, 6, 8, 10, and 12 weeks of age. Four non-linear models (Gompertz, Logistic, von Bertalanffy, and Brody) were used to fit the MeL and MeC growth curves. Subsequently, the estimated growth curve parameters of the mature MeL or MeC (**A**), time-scale parameter (**b**), and maturity rate (**K**) from the non-linear models were utilized as substitutes for the original bone data in GWAS. The Logistic and Brody models displayed the best goodness-of-fit for MeL and MeC, respectively. Single-trait and multi-trait GWASs based on the growth curve parameters of the Logistic and Brody models revealed 4 618 significant single nucleotide polymorphisms (**SNPs**), annotated to 332 genes, associated with metatarsal bone traits. The majority of these significant SNPs were located on *Gallus gallus* chromosome (**GGA**) 1 (167.433–176.31 8 Mb), GGA2 (96.791–103.543 Mb), GGA4 (65.003–83.104 Mb) and GGA6 (64.685–95.285 Mb). Notably, we identified 12 novel GWAS loci associated with chicken metatarsal bone traits, encompassing 35 candidate genes. In summary, the combination of single-trait and multi-trait GWASs based on growth curve parameters uncovered numerous genomic regions and candidate genes associated with chicken bone traits. The findings benefit an in-depth understanding of the genetic architecture underlying metatarsal growth and development in chickens.

Implications

Chicken bones play an important role in supporting and protecting the body, and have a vital impact on actual production. In this study, we used Logistic and Brody models to describe the growth curves of metatarsal length and circumference in F_2 chickens. Furthermore, our analysis identified 51 known genes related to bone traits and 12 novel genomic regions (encompassing 35 genes) that may affect chicken bone growth and development. These findings enhance our understanding of the growth patterns and genetic determinants of bone traits in chickens and may aid selective breeding programs in the future.

Introduction

The skeletal system is crucial for poultry birds because it serves multiple vital functions, such as body protection and support. Moreover, the bones also act as reservoirs of calcium/phosphorus and house the organism's bone marrow (Aguado et al., 2015). Due to various genetic and environmental factors, chickens often develop several bone disorders and injuries, including osteoporosis, fractures, and chondrodysplasia (De Koning et al., 2020; Li

* Corresponding author.
E-mail address: lihui@neau.edu.cn (H. Li).
[1] These authors equally contributed to this work.

https://doi.org/10.1016/j.animal.2024.101129
1751-7311/

et al., 2021b; Johnsson et al., 2023). These disorders not only result in significant economic losses to the poultry industry but also endanger animal welfare (Jansen et al., 2020). The main causes of these disorders and injuries among chickens are the paucity of space for exercise, the mechanical stress on bones, and excessive weight gain without a corresponding increase in bone strength for support (Dale et al., 2015; Guo et al., 2020). In addition to nutrition and housing, genetic factors also contribute to bone traits in chickens (Fleming et al., 2006; Jansen et al., 2020). Therefore, some of these aforementioned health issues can be addressed via genetic improvements.

In recent years, with the development of single-nucleotide polymorphism (**SNP**) arrays and sequencing technologies, a large number of SNP markers have become available. Genome-wide association study (**GWAS**), which is based on high-density SNP markers, has emerged as one of the most commonly used strategies for identifying genes associated with complex traits (Chang et al., 2018). So far, an array of genomic regions and genes related to chicken bone traits has been identified using GWAS. Previously, Zhang et al. (2020) studied growth traits in chickens based on haplotype GWAS and identified six candidate genes associated with bone development. Further, Li et al. (2021b) used GWAS and selective signature analysis to uncover 21 candidate genes related to chicken bone growth and development. In addition, by employing GWAS for the genetic analysis of bone strength, bone mineral density, and bone composition in 860 commercial hybrid laying hens, Johnsson et al. (2023) found three loci associated with bone length.

In animals, growth as a quantitative trait can simply be defined as the change in body size per unit of time (Narinç et al., 2017). Longitudinal traits are typically those whose phenotypic values change over time (Kellogg et al., 2014). In contrast to conventional single-record phenotypic traits, longitudinal traits provide a more comprehensive representation of growth and production patterns in animals. Notably, such data are usually analyzed using fitted growth curves (Ning et al., 2018; Oliveira et al., 2019; Duan et al., 2021). Non-linear models systematically describe the growth of animals based on several parameters (Aggrey, 2002; Lee et al., 2020; Seifi Moroudi et al., 2021), such as mature traits (A), time-scale parameters (b), and the maturation rate (K), which measures the characteristics of individuals throughout their developmental period. Non-linear models such as the Gompertz, Logistic, von Bertalanffy, and Brody models have been widely used to describe the growth curves of chickens (Xie et al., 2020; Nguyen et al., 2021). Several researchers have also studied the growth curves of different native breeds of chickens (Mata-Estrada et al., 2020; Boonkum et al., 2021; Nguyen Hoang et al., 2021), providing insights essential for understanding the growth and development patterns of chickens, and thereby improving local breeds and feeding management strategies.

More recently, many candidate genes related to growth traits have been identified by GWAS based on growth curve parameters in agricultural economic animals. Compared with the traditional GWAS input value based on the raw phenotype at a certain time point, the advantages of the growth curve parameter as GWAS input are to reflect the changes of traits with time (Wang et al., 2022), eliminate the influences of some experimental errors (Mignon-Grasteau et al., 1999), improve the interpretability of biology (Soares et al., 2017). Studies in beef cattle have identified several candidate genes associated with growth and development using GWAS based on the growth curve parameters of BW (Crispim et al., 2015; Duan et al., 2021). However, so far, there has only been one such study on GWAS based on growth curve parameters in chickens. In this study, Seifi Moroudi et al. (2021) estimated the growth curve parameters of chicken BW using the Gompertz model, and based on GWAS, they found that *GH*, *RET*, *GRB14*, and *FTAJ3* may be related to growth and meat quality in chickens. No one has yet used this method to study bone traits in chickens.

To this end, the present study aimed to evaluate the growth curve models of metatarsal length (**MeL**) and metatarsal circumference (**MeC**) in chickens at five growth stages. Further, we screened candidate genomic regions and genes associated with metatarsal bone traits using a combination of single-trait and multi-trait GWASs based on optimal growth curve parameters. The findings could help in elucidating the genetic basis underlying metatarsal bone growth and development in chickens.

Material and methods

Experimental populations and phenotypic measurements

The Northeast Agricultural University Resource Population was used in the current study. This F_2 population was generated by crossing broiler sires, derived from a line selected for high abdominal fat content, with Baier layer dams (a Chinese native breed) (Leng et al., 2009). More details regarding this line have been provided in previous reports (Zhang et al., 2010 and 2011). A total of 471 F_2 individuals (243 males and 228 females) from 12 half-sib families were examined in this study. All the chickens were raised under the same environmental conditions. They had free access to feed and water, and received corn and soy-based commercial feeds in accordance with all requirements of the NRC (1994). From hatching to 3 weeks of age, the chickens were maintained on an initial diet (metabolizable energy, 3 000 kcal/kg; CP, 210 g/kg). Subsequently, from 4 to 12 weeks of age, the chickens were fed a growth diet (metabolizable energy, 3 100 kcal/kg; CP, 190 g/kg). The MeL and MeC values of all F_2 chickens were measured every 2 weeks between 4 and 12 weeks of age. MeL was measured as the straight-line distance from the superior metatarsal joint to the third and fourth toes. Meanwhile, MeC was measured using a thin piece of string around the middle metatarsus, and the length of the string was then measured using sliding calipers. In the process of measuring metatarsal length and metatarsal circumference, the experimenter laid the chicken on its side on the table and fixed the chicken's position with both hands, another experimenter then measured the chickens for MeL and MeC (Supplementary Figure S1).

Genotyping and quality control

Total genomic DNA was extracted from the blood of each chicken using a reagent test kit. Then, a total of 26 F_0 (ancestors of F_2 chickens) and 471 F_2 individuals were used for genome sequencing on the Illumina HiSeq PE150 platform. The average depth of re-sequencing was 10 $\times$ for F_0 individuals and 3 $\times$ for F_2 individuals. Library construction and sample indexing were performed according to standard Illumina protocols. Paired-end reads were mapped to the GCF_000002315.6_GRCg6a reference genome using Burrows-Wheeler Aligner (**BWA**) (version: 0.7.8) (Li and Durbin, 2009), the command line was "BWA mem -t 4 -k 32 -M". After alignment, SNP calling was performed on a population scale using a Bayesian approach, as implemented in the package SAMtools (Li et al., 2009). Subsequently, we calculated genotype likelihoods from reads for each individual at each genomic location, and we examined the allele frequencies in the sample through a Bayesian approach. Only high-quality SNPs (coverage depth $\geq$ 2, root mean square (RMS) mapping quality $\geq$ 20, and miss $\leq$ 0.3) were retained for subsequent analysis to exclude SNP calling errors due to incorrect mapping (Huang et al., 2019).

Among the 15 868 916 raw SNPs, only 10 889 955 SNPs remained after filtering. The missing genotypes in the 471 individ-

uals of the F_2 generation were imputed through a 10 × cross-validation of sequencing data from the F_0 generation. Imputation was performed using BEAGLE 4.0 with default parameter settings (Browning and Browning, 2009). Then, after further quality control (based on MAF ≥ 0.05 and miss ≤ 0.2), 7 855 035 of the 10 889 955 SNPs imputed were retained.

Growth curve fitting

Four widely used non-linear models were fitted individually to the MeL and MeC records of global, male, and female chickens. The equations, including parameters for each model, were summarized in Table 1. These models were fitted for each individual using the iterative non-linear least squares method via the Gauss-Newton algorithm implemented with the *nlme* (non-linear mixed-effects model) package of R software (Heisterkamp et al., 2017). The following standard statistics were utilized to compare the models: **R^2**, Akaike's information criterion (**AIC**), Bayesian information criterion (**BIC**), and **RMSE**. The respective formulas for each were as follows: 1): $R^2 = 1 - (SS_E / SS_T)$; 2): $AIC = n \times \ln(SS_E / n) + 2k$; 3): $BIC = n \times \ln(SS_E / n) + k \times \ln(n)$, and 4): $RMSE = \sqrt{\frac{RSS}{n-p-1}}$, where SS_E is the sum of squares of errors, SS_T is the total sum of squares, n is the number of observations, k is the number of parameters, ln is the natural logarithm, RSS is the residual sum of squares, and p is the number of parameters in the equation (Mokhtari et al., 2019; Mata-Estrada et al., 2020).

Genome-wide association study based on growth curve parameters

After selecting the non-linear models that best fit the MeL and MeC traits, the parameters of the mature MeL or MeC (**A**), time-scale parameter (**b**), and maturity rate (**K**) were used for single-trait and multi-trait GWASs. Association analysis was conducted using the GEMMA (Genome-wide Efficient Mixed-model Association) software package (Zhou and Stephens, 2012). For the Linear Mixed Model analysis, the equation was as follows:

$$Y = W\alpha + X\beta + S\mu + e$$

Here, for single-trait GWAS, Y represents the vector of the phenotypic values (A, b and K estimates) of each individual; W is the incidence matrix of fixed effects; α is the vector of corresponding coefficients including the intercept. Notably, sex is included as a fixed effect to build up the W matrix. Moreover, X represents the vector of marker genotypes and β is the corresponding effect of the marker. S is the incidence matrix for μ, and μ is the vector of random additive genetic effects following the multinormal distribution $N(0, G\sigma^2_\mu)$, in which G is the genomic relationship matrix based on identity by state (IBS), and σ^2_μ is the polygenetic additive variance. Finally, e represents the random residual with a distribution of $N(0, I\sigma^2_e)$ (such that I is a n by n identity matrix, and n is the number denoting the individual).

For multi-trait GWAS in this study, the multi-trait GWAS means that three parameters of the curve analysis were used as three genetic traits and fitted simultaneously into three-trait GWAS analysis. Meanwhile, Y is an n by d matrix of d phenotypes for n individuals; W is the incidence matrix of covariates (fixed effects); and α is a c by d matrix of the corresponding coefficients including the intercept, in which c represents the number of covariates. Here, sex used for population structure correction is included as a covariate to build up the W matrix. Moreover, X represents the vector of marker genotypes, and β is a d vector of marker effect sizes for the d phenotypes. Additionally, S is the incidence matrix for μ. And μ is an n by d vector of random additive genetic effects following the multinormal distribution $MN_{n\times d}(0, K, V_g)$, in which K is the genomic relationship matrix, V_g is a d by d symmetric additive genetic variance–covariance matrix. e represents an n by d matrix of random residuals with a distribution of $MN_{n\times d}(0, I_{n\times n}, V_e)$. Of note, $I_{n\times n}$ is a n by n identity matrix, V_e is a d by d symmetric matrix of the environmental variance component. Due to the fact that the traits represent measurements on the same individuals, we modeled the environmental components as correlated: $Ve = Var\begin{bmatrix} e_{1i} \\ e_{2i} \\ e_{3i} \end{bmatrix} = \begin{bmatrix} \sigma^2_{e1} & \sigma_{e12} & \sigma_{e13} \\ \sigma_{e12} & \sigma^2_{e2} & \sigma_{e23} \\ \sigma_{e13} & \sigma_{e23} & \sigma^2_{e3} \end{bmatrix}$.

We performed principal component (**PC**) analysis (**PCA**) on the F_2 population, and the results are shown in Supplementary Figure S2. Importantly, no separate clusters were identified in this population, indicating that the experimental population was not significantly stratified. Therefore, PCs were not ultimately included in the mixed model. Also, we calculated the observed heterozygosity (H_o) and expected heterozygosity (H_e) to perform genetic diversity analysis of the genome using '--het' of PLINK software (version 1.9) (Purcell et al., 2007). The average H_o was 0.312, and the H_e was 0.302, which indicated that the genetic diversity of this population was rich. A relatively stringent threshold was set as $P < 1.0 \times 10^{-6}$ to control the genome-wide type 1 error rate according to the study by Ma et al. (2018), which is easy to compare with our previous work. Finally, association results were plotted using CMplot software (Yin et al., 2021).

Single nucleotide polymorphism functional annotation and quantitative trait loci overlapping

SNP annotation was performed for all screened loci associated with growth curve parameters according to the GCF_000002315.6_GRCg6a reference genome using the package ANNOVAR (Version: 2013-05-20) (Wang et al., 2010). Only SNPs significantly associated with traits were annotated, and candidate genes were identified according to their physical location on the *Gallus gallus* chromosome (**GGA**) and biological function. Based on linkage disequilibrium (**LD**) decay distance analysis in previous studies (genome distance spans 40 kb when the r^2 drops to 0.1) (Li et al., 2021b), the candidate genes in the 40-kb upstream and downstream regions of each top SNP were screened. Functional enrichment was analyzed based on Gene Ontology (**GO**) and Kyoto Encyclopedia of Genes and Genomes (**KEGG**) using the OmicShare tool (https://www.omicshare.com/tools/), and candidate genes were functionally annotated by referring to relevant literature reports. Furthermore, The Animal Quantitative Trait Loci (**QTL**) database (**Animal QTLdb**, https://www.animalgenome.org/cgi-bin/QTLdb/GG/index, updated on 25 April 2023) was searched for the locations of significant SNPs to determine whether these SNPs had previously been reported as QTLs.

Table 1
Non-linear regression models were fitted to the growth curves for chicken metatarsal length and metatarsal circumference.

Models	Function	Number of parameters
Gompertz	$W = Aexp(-bexp^{-Kt})$	3
Logistic	$W = A(1 + bexp^{-Kt})^{-1}$	3
von Bertalanffy	$W = A(1\text{-}bexp^{-Kt})^3$	3
Brody	$W = A(1\text{-}bexp^{-Kt})$	3

Abbreviations: W = the metatarsal length (MeL) or metatarsal circumference (MeC) reached to age t; A = the mature MeL or MeC; b = time-scale parameter; K = maturity rate; t = growth time; exp = the exponential. Model codes are available in Supplementary Material S1.

Table 2
The descriptive statistics of metatarsal length (MeL) and metatarsal circumference (MeC) in chickens.

Traits	Category	Weeks	Number of animals	Mean (cm)	SD	Min (cm)	Max (cm)
MeL	Global	4	471	5.69	0.35	4.12	6.97
	Male	4	243	5.87	0.29	4.81	6.97
	Female	4	228	5.50	0.31	4.12	6.29
MeL	Global	6	471	7.12	0.46	5.47	8.39
	Male	6	243	7.40	0.36	6.40	8.39
	Female	6	228	6.83	0.37	5.47	8.01
MeL	Global	8	471	8.53	0.63	6.74	10.17
	Male	8	243	8.96	0.47	7.45	10.17
	Female	8	228	8.08	0.44	6.74	9.41
MeL	Global	10	471	9.35	0.77	7.20	11.45
	Male	10	243	9.94	0.48	8.40	11.45
	Female	10	228	8.73	0.46	7.20	10.06
MeL	Global	12	471	9.90	1.02	7.52	13.70
	Male	12	243	10.73	0.58	8.56	13.70
	Female	12	228	9.03	0.51	7.52	10.73
MeC	Global	4	471	3.07	0.22	2.30	3.70
	Male	4	243	3.18	0.19	2.65	3.70
	Female	4	228	2.96	0.19	2.30	3.45
MeC	Global	6	471	3.85	0.27	3.20	4.65
	Male	6	243	4.02	0.21	3.35	4.65
	Female	6	228	3.68	0.20	3.20	4.15
MeC	Global	8	471	4.01	0.33	3.25	5.05
	Male	8	243	4.23	0.25	3.60	5.05
	Female	8	228	3.77	0.22	3.25	4.65
MeC	Global	10	471	4.17	0.36	3.30	5.30
	Male	10	243	4.43	0.26	3.75	5.30
	Female	10	228	3.89	0.23	3.30	4.60
MeC	Global	12	471	4.32	0.40	3.30	5.80
	Male	12	243	4.62	0.28	3.85	5.80
	Female	12	228	4.01	0.24	3.30	4.70

Abbreviations: Min = minimum; Max = maximum.

Table 3
Estimated values of growth curve parameters and goodness-of-fit assessments for the non-linear models in chickens.

Models	Traits	Category	Parameters			Goodness-of-fit[1]			
			A (cm)	B	K	R^2	AIC	BIC	RMSE
Gompertz	MeL	Global	11.083	1.673	0.228	0.832	−1750.460	−1733.168	0.689
		Male	12.606	1.692	0.197	0.938	−1923.971	−1908.664	0.453
		Female	9.693	1.711	0.277	0.902	−1921.639	−1906.523	0.430
Logistic	MeL	Global	10.697	3.005	0.304	0.833	−1758.641	−1741.348	0.688
		Male	11.946	3.166	0.277	0.938	−1931.251	−1915.944	0.451
		Female	9.496	2.936	0.345	0.909	−1934.266	−1919.150	0.428
von bertalanffy	MeL	Global	11.263	0.461	0.202	0.832	−1747.049	−1729.756	0.690
		Male	12.938	0.460	0.170	0.937	−1920.490	−1905.182	0.453
		Female	9.779	0.479	0.249	0.902	−1916.863	−1901.746	0.431
Brody	MeL	Global	11.758	0.956	0.152	0.831	−1739.282	−1721.989	0.691
		Male	13.938	0.930	0.117	0.937	−1912.057	−1896.750	0.455
		Female	9.995	1.022	0.203	0.901	−1906.574	−1891.457	0.433
Gompertz	MeC	Global	4.285	2.266	0.484	0.635	−5262.905	−5245.613	0.327
		Male	4.608	1.984	0.423	0.802	−3402.087	−3386.780	0.246
		Female	3.952	3.084	0.596	0.730	−3439.646	−3424.530	0.221
Logistic	MeC	Global	4.272	3.314	0.540	0.633	−5254.401	−5237.108	0.328
		Male	4.588	2.950	0.480	0.801	−3391.198	−3375.890	0.247
		Female	3.945	4.465	0.654	0.729	−3434.573	−3419.457	0.222
Von bertalanffy	MeC	Global	4.290	0.668	0.466	0.635	−5265.658	−5248.366	0.327
		Male	4.615	0.581	0.405	0.803	−3405.580	−3390.273	0.246
		Female	3.954	0.912	0.577	0.730	−3441.327	−3426.211	0.221
Brody	MeC	Global	4.300	1.575	0.430	0.636	−5271.023	−5253.730	0.326
		Male	4.632	1.355	0.369	0.804	−3412.335	−3397.027	0.245
		Female	3.959	2.168	0.541	0.731	−3444.660	−3429.544	0.221

Abbreviations: MeL = metatarsal length; MeC = metatarsal circumference; A = the mature MeL or MeC; b = time-scale parameter; K = maturity rate; AIC = Akaike's information criterion; BIC = Bayesian information criterion.
[1] The preferred model is the one with the smallest AIC, BIC and RMSE values, and the biggest R^2 values.

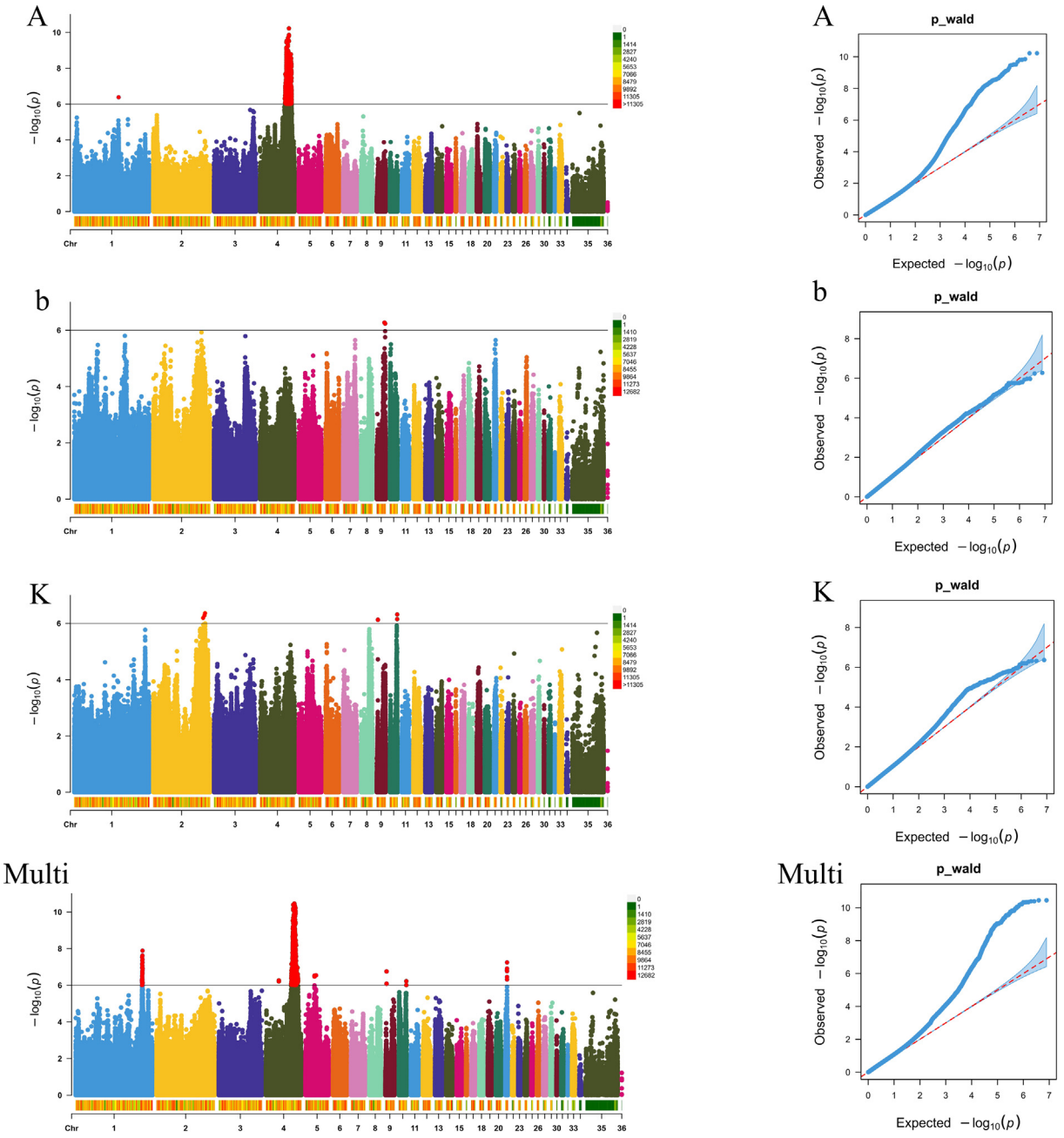

Fig. 1. Manhattan plot with marker density information and quantile–quantile (Q–Q) plot for the single-trait, multi-trait genome-wide association study (GWAS) based on growth curve parameters (A = the mature MeL or MeC; b = time-scale parameter; K = maturity rate) of metatarsal length (MeL) in chickens. In the Manhattan plot (left), single nucleotide polymorphisms (SNPs) on different chromosomes (chromosomes Z and W were shown as 35 and 36, respectively) were denoted by different colors; marker density was shown at the bottom of the Manhattan plot; the horizontal black line presented significant genome-wide association threshold ($P = 1.0 \times 10^{-6}$). Q-Q plots were displayed as scatter plots of observed and expected log *P*-values (right).

Results

Growth curve fitting

Descriptive statistics of recorded MeL and MeC values are presented in Table 2. The fitted parameters of the four MeL and MeC growth curve models are shown in Table 3. For MeL, the Logistic model was found to be the most optimal because it had the highest R^2 values (global = 0.833, males = 0.938, females = 0.909) and the lowest AIC, BIC, and RMSE values (for global, males, and females) among all the models. For MeC, the Brody model was found to be the most optimal because it had the highest R^2 values (global = 0.636, males = 0.804, females = 0.731) and the lowest AIC, BIC, and RMSE values (for global, males, and females). Therefore, the Logistic and Brody models were considered the most appropriate for describing the growth trajectory of MeL and MeC in chickens, respectively.

Genome-wide association study based on growth curve parameters

Before doing GWAS, we calculated the heritability and genetic correlation of the estimated growth curve parameters of MeL and MeC. The strong genetic correlations among the parameters are observed, varying from −0.605 to 0.919 (Supplementary Table S1), which illustrates that it is appropriate to perform multi-trait GWAS. Figs. 1 and 2 show the Manhattan plots and

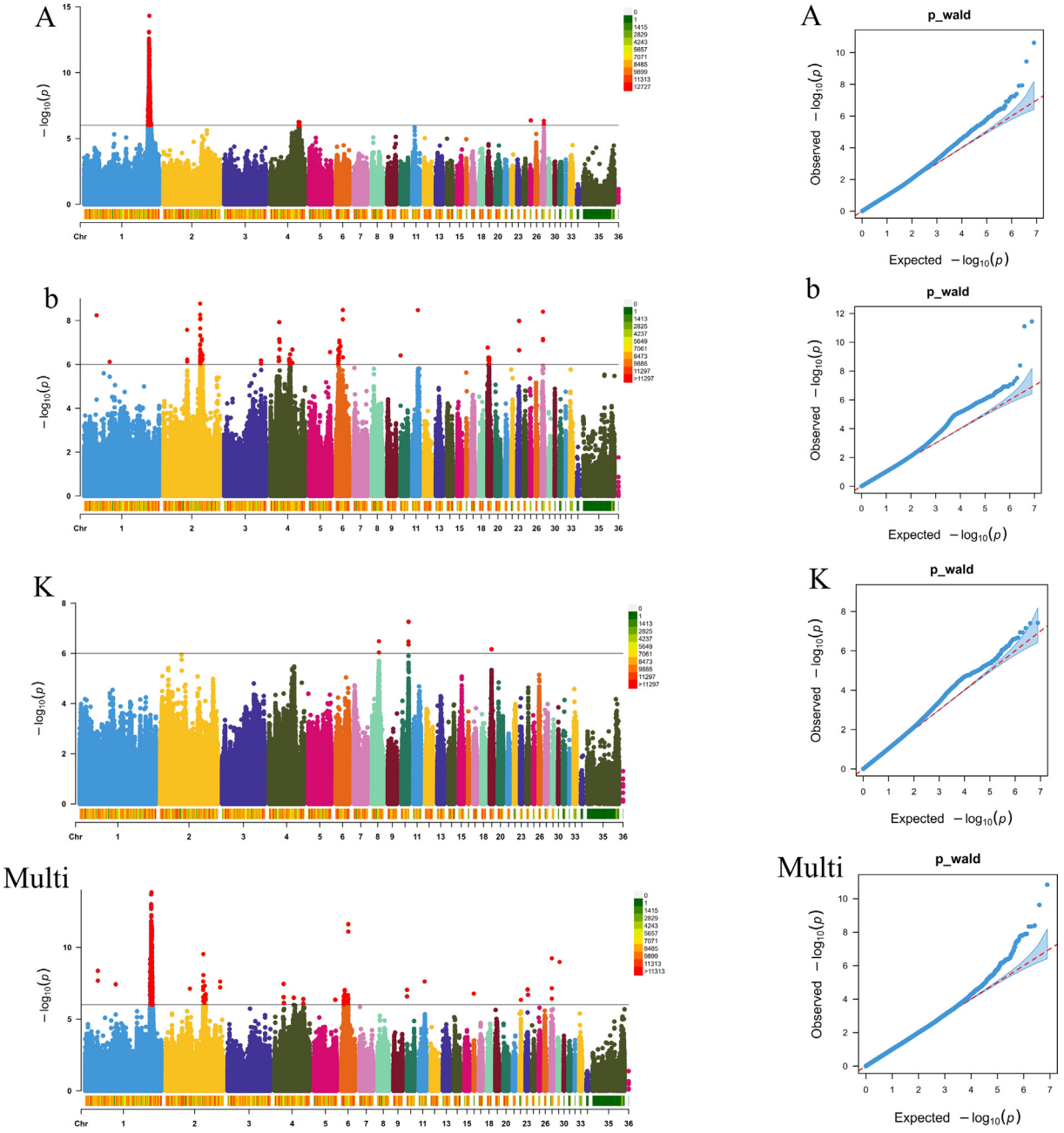

Fig. 2. Manhattan plot with marker density information and quantile–quantile (Q–Q) plot for the single-trait, multi-trait genome-wide association study (GWAS) based on growth curve parameters (A = the mature MeL or MeC; b = time-scale parameter; K = maturity rate) of metatarsal circumference (MeC) in chickens. In the Manhattan plot (left), single nucleotide polymorphisms (SNPs) on different chromosomes (chromosomes Z and W were shown as 35 and 36, respectively) were denoted by different colors; marker density was shown at the bottom of the Manhattan plot; the horizontal black line presented significant genome-wide association threshold ($P = 1.0 \times 10^{-6}$). Q-Q plots were displayed as scatter plots of observed and expected log *P*-values (right).

quantile–quantile (**Q-Q**) plots of MeL and MeC growth curve parameters for single-trait and multi-trait GWASs, respectively. The Q-Q plots were employed to estimate the variance between observed and expected chi-square statistic values of metatarsal bone traits. The plots indicated that the potential candidate loci associated with these traits did not arise due to population stratification. Additionally, genomic inflation factors for A and Multi of MeL in Fig. 1 were 0.960 and 1.165, respectively, indicating that there is no stratification. Thus, the statistical model employed for this experiment was reasonable.

Single-trait and multi-trait genome-wide association study for metatarsal length

Single-trait GWAS revealed 1 337 significant SNPs related to A (the mature MeL), for these SNPs, we found that most of them were not in high LD ($R^2 \leq 0.6$), and a few SNPs were high LD ($R^2 > 0.6$) (Supplementary Figure S3). An overwhelming majority of these significant SNPs were located on GGA4, within the 65.006–83.104 Mb genomic region. The SNP with the lowest *P*-value was located at 76 028 664 bp on GGA4 (Fig. 1A). For b (time-scale parameter), two significant SNPs were located on GGA9, and the

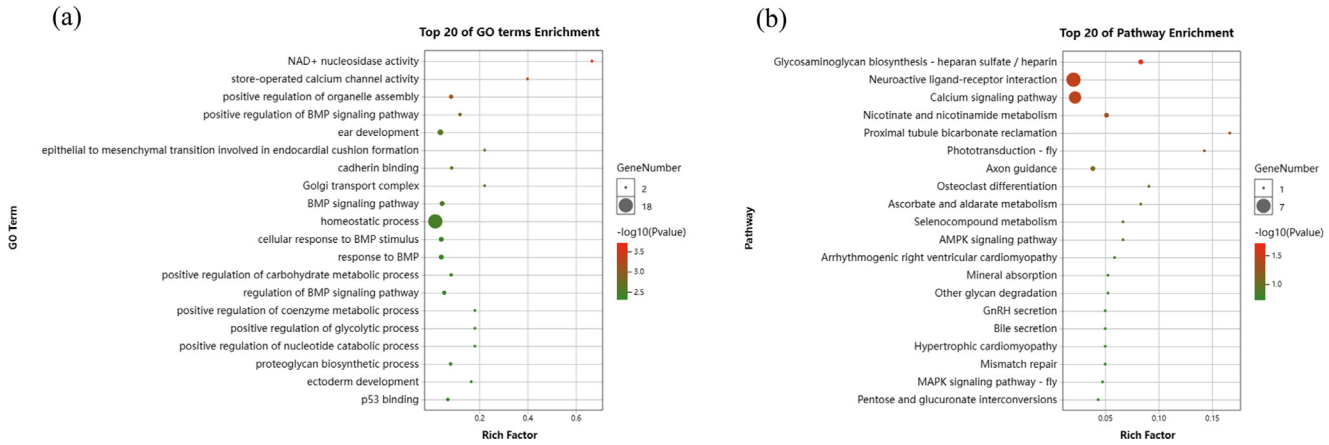

Fig. 3. Gene Ontology (GO) and Kyoto Encyclopedia of Genes and Genomes (KEGG) enrichment analysis of candidate genes in chickens. Fig. 3a showed the top 20 enriched GO terms for bone traits. Fig. 3b showed the top 20 pathway enrichments for bone traits. Rich factor refers to the ratio of the number of genes with the term entry with respect to the total number of genes in the term entry. The larger the rich factor, the higher the degree of enrichment. The bubble size indicates the number of genes, and the color of the bubble indicates the level of significance.

SNP with the lowest *P*-value was located at 20 906 955 bp on GGA9 (Fig. 1b). Regarding K (maturity rate), there were nine significant SNPs on GGA2, GGA9, and GGA10, and the SNP with the lowest *P*-value was located at 136 414 685 bp on GGA 2 (Fig. 1K). Meanwhile, 1 077 significant SNPs were identified on multi-trait GWAS, and these were mainly located on GGA1, GGA4, GGA5, GGA9, GGA10, and GGA21. The lead SNP was located at 73 074 342 bp on GGA 4 (Fig. 1Multi). Overall, the annotation of significant SNPs indicated that 178 genes were associated with MeL during growth and development in chickens, including *DMD*, *FOXO1*, *TEC*, *CORIN*, and *PCDH7* (Supplementary Table S2).

Single-trait and multi-trait genome-wide association study for metatarsal circumference

In the single-trait GWAS, 2 598 significant SNPs associated with A (the mature MeC) were detected, and these were distributed on GGA1, GGA4, GGA25, and GGA27. Likewise, for these SNPs, we found that most of them were not in high LD ($R^2 \leq 0.6$), and a few SNPs were high LD ($R^2 > 0.6$) (Supplementary Figure S4). The SNP with the lowest *P*-value was located at 171 411 019 bp on GGA1 (Fig. 2A). For b (time-scale parameter), a total of 115 significant SNPs were identified, and the SNP with the lowest *P*-value was located at 96 941 984 bp on GGA2 (Fig. 2b). Meanwhile, seven significant SNPs distributed on GGA8, GGA10, and GGA19 were identified for K (maturity rate), and the SNP with the lowest *P*-value was located at 19 462 192 bp on GGA10 (Fig. 2K). Meanwhile, in the multi-trait GWAS, 1 872 significant SNPs were identified, and the top SNP was located at 171 411 019 bp on GGA1 (Fig. 2Multi). The annotation of significant SNPs revealed 173 genes associated with skeletal development, such as *RB1*, *EXOSC8*, *LHFP*, *TPT1*, and *TRPC4* (Supplementary Table S3).

Candidate genes, functional enrichment analysis, and comparison with known quantitative trait loci

We collated all the annotated genes from the GWAS to explore their functions in terms of bone growth and development in chickens. In total, 332 genes were analyzed for functional enrichment (Supplementary Table S4). A bubble chart showing the GO enrichment results of these genes is presented in Fig. 3a. The genes were mainly enriched in GO terms related to the store-operated calcium channel activity, positive regulation of the BMP signaling pathway, and homeostatic processes. These genes were enriched for 22 biological processes, nine molecular functional, and 14 cellular component modules (Supplementary Figure S5). The KEGG analysis demonstrated that these candidate genes were involved in the calcium signaling pathway and in osteoclast differentiation (Fig. 3b).

In order to further screen for candidate genes related to bone growth and development traits, we explored the genes related to the regulation of animal or human bone development and differentiation based on the NCBI database and the current literature. Based on the literature, we identified 51 candidate genes implicated in the regulation of bone mineral density, bone homeostasis, bone cell proliferation, and differentiation and remodeling (Table 4). In addition, we compared the physical locations of the significant SNPs identified using single-trait and multi-trait GWASs with known QTLs for bone traits (Animal QTLdb). Accordingly, we discovered 12 novel QTL regions encompassing 35 candidate genes related to metatarsal bone growth and development in chickens (Table 5 and Supplementary Table S4).

Discussion

The growth rate of broiler chickens has improved significantly in the last few decades. However, the lack of corresponding skeletal growth and development has resulted in an increase in health issues among chickens, because the bones are incapable of supporting their BW (Li et al., 2021b). The development of the chicken skeleton is influenced by nutritional, housing, and genetic factors, with genetics having a major influence (Fleming et al., 2006). Hence, this study was designed to dissect the genetic determinants underlying metatarsal bone growth and development in chickens based on a combination of growth curve parameters and GWAS.

Growth curve fitting

Organismal growth and development follow sigmoid trends, enabling the use of mathematical non-linear models for describing growth patterns (Hojjati and Ghavi Hossein-Zadeh, 2018). An ideal growth curve model can predict the dynamics of poultry growth and development to guide daily feed management. Furthermore, it can also integrate a range of phenotypic values into its parameters and thereby effectively eliminate the effects of some experimental errors (Mignon-Grasteau et al., 1999).

In the present study, four non-linear models were applied to fit the growth curves of the MeL and MeC traits in an F_2 chicken population. According to goodness-of-fit criteria, the Logistic model was superior to the other three models for the MeL trait. The

Table 4
Candidate genes for bone traits that were identified by genome-wide association study (GWAS) based on growth curve parameters in chickens.

Genes	Description	Chr	Position (bp)	Literature evidence
SPX	spexin hormone	1	67 109 142	Increased bone regeneration (Assefa et al., 2022)
DMD	dystrophin	1	116 825 716	Decreases skeletal homeostasis (Li et al., 2021a)
VWA8	von Willebrand factor A domain containing 8	1	167 433 170	Serum calcium, bone mineral density (Cerani et al., 2019)
TPT1	tumor protein, translationally-controlled 1	1	169 087 184–169 092 662	Related to differentiation and proliferation of osteoclasts (Choi et al., 2014)
LCP1	lymphocyte cytosolic protein 1	1	169 398 661	Correlated with lumbar volumetric bone mineral density (Alam et al., 2010)
LRCH1	leucine rich repeats and calponin homology domain containing 1	1	169 463 574–169 493 854	Associated with osteoarthritis (Snelling et al., 2007)
HTR2A	5-hydroxytryptamine receptor 2A	1	169 663 240–169 698 740	Affects bone size and mass (Guo et al., 2020)
RB1	RB transcriptional corepressor 1	1	170 082 414–170 149 466	Inhibits bone formation and remodeling (Li et al., 2022)
LPAR6	lysophosphatidic acid receptor 6	1	170 118 168	Affects bone size and mass (Guo et al., 2020)
FNDC3A	fibronectin type III domain containing 3A	1	170 278 593–170 430 150	Regulates bone growth and development (Li et al., 2021b)
CAB39L	calcium binding protein 39 like	1	170 464 682–170 526 612	Affects bone size and mass (Guo et al., 2020)
FOXO1	forkhead box O1	1	171 878 547––172 002 903	Promotes osteoblast proliferation and differentiation (Huang et al., 2023)
LHFP	lipoma HMGIC fusion partner-like 1	1	172 271 856–172 460 529	Regulator of osteoblast activity and bone mass (Mesner et al., 2019)
TRPC4	transient receptor potential cation channel subfamily C member 4	1	173 088 952–173 255 286	Affects bone size and mass (Guo et al., 2020)
POSTN	Periostin	1	173 393 314–173 433 539	Plays an important role in periosteal bone formation (Gardinier et al., 2023)
EXOSC8	exosome component 8	1	173 692 028–173 700 538	Affects osteogenic differentiation of mesenchymal stem cells (Yang et al., 2019)
SMAD9	SMAD family member 9	1	173 722 552–173 774 897	Regulates bone growth and development (Li et al., 2021b)
SULT1E1	sulfotransferase family 1E member 1	4	51 813 628	Relates to bone mineral density (Lee et al., 2006)
EGF	epidermal growth factor	4	58 030 684	Promotes bone formation (Basal et al., 2018)
NMU	neuromedin U	4	65 006 329	Suppresses osteoblast differentiation and activity (Born-Evers et al., 2023)
KDR	kinase insert domain receptor	4	65 233 938	Relates to bone mineral density (Han et al., 2022)
TEC	tec protein tyrosine kinase	4	66 502 721–66 544 891	Involved in osteoclast differentiation and activation (Ariza et al., 2019)
CORIN	corin, serine peptidase	4	66 706 462	Promotes endochondral ossification and bone development (Nordberg et al., 2018)
SHISA3	shisa family member 3	4	68 245 369–68 280 140	Promotes the development of osteoblasts (Murakami et al., 2019)
PCDH7	protocadherin 7	4	71 564 618–71 797 291	Regulates the formation of osteoclasts and contributes to the maintenance of bone homeostasis (Kim et al., 2020)
STIM2	stromal interaction molecule 2	4	73 033 422–73 139 299	Regulates both intracellular Ca^{2+} distribution and Ca^{2+} movement in skeletal muscle (Oh et al., 2017)
RBPJ	recombination signal binding protein for immunoglobulin kappa J region	4	73 215 916–73 363 088	Negative regulation of osteoclast formation (Li et al., 2014)
SLC34A2	solute carrier family 34 member 2	4	73 419 064–73 471 857	Decreased bone mineral density and increased number of osteoclasts (Knöpfel et al., 2017)
PPARGC1A	PPARG coactivator 1 alpha	4	73 797 784–74 076 981	Promotes differentiation of osteoblasts (Yu et al., 2018)
ADGRA3L	adhesion G protein-coupled receptor A3	4	74 443 278–74 526 009	Positively regulates osteoclast formation (Tang et al., 2022)
SLIT2	slit guidance ligand 2	4	75 110 352–75 247 724	Inhibits osteoclastogenesis and bone resorption (Park et al., 2019)
MED28	mediator complex subunit 28	4	75 970 316–75 970 696	Associated with bone weight (Niu et al., 2021)
LAP3	leucine aminopeptidase 3	4	75 974 422–75 975 267	Associated with bone weight (Miao et al., 2018; Niu et al., 2021)
TAPT1	Transmembrane anterior posterior transformation 1	4	76 464 567–76 502 119	Skeletal dysplasias (Symoens et al., 2015)
FGFBP1	fibroblast growth factor binding protein 1	4	76 597 691–76 599 976	Associated with Bone Mineral Density and osteoporosis (Hoppman et al., 2010)

Table 4 (*continued*)

Genes	Description	Chr	Position (bp)	Literature evidence
CD38	CD38 molecule	4	76 597 691–76 599 976	Regulation of cartilage differentiation disrupts cartilage homeostasis (Ma et al., 2022)
BST1	bone marrow stromal cell antigen 1	4	76 651 477	Positive regulation of the potential for osteogenic differentiation of human mesenchymal stem cells (hMSCs) (Aomatsu et al., 2014)
NKX3-2	NK3 homeobox 2	4	77 422 730–77 438 511	Inhibits chondrocyte maturation (Waldmann et al., 2021)
MSX1	msh homeobox 1	4	78 806 517–78 806 811	Regulates the differentiation of osteoblasts (Goto et al., 2016)
CYTL1	cytokine- like 1	4	78 880 639–78 899 473	Involved in chondrogenesis and maintenance of cartilage metabolism (Zhu et al., 2020)
EVC2	EvC ciliary complex subunit 2	4	79 065 293–79 088 624	Affects the Cranial Bone Development (Kwon et al., 2018)
AFAP1	actin filament- associated protein 1	4	80 616 404	Induction of osteoblast differentiation (Cho et al., 2015)
ABLIM2	actin binding LIM protein family member 2	4	80 616 404–80 776 526	Related to osteoporosis (Cheishvili et al., 2018)
CPZ	carboxypeptidase Z	4	81 170 000–81 395 990	Regulates bone growth and development (Li et al., 2021b)
RGS12	regulator of G-protein signaling 12	4	82 013 271	Promotes osteoclast production (Yuan et al., 2022)
FAM193A	family with sequence similarity 193, member A	4	82 511 483	Associated with osteoporosis (Lee et al., 2019)
RNF4	ring finger protein 4	4	82 594 684–82 594 969	Promotes osteoblast differentiation (Novak et al., 2022)
GLCE	glucuronic acid epimerase	10	19 757 194–19 761 232	Influence on cartilage homeostasis (Chanalaris et al., 2019)
CASZ1	castor zinc finger 1	21	3 987 089–4 036 096	Associated with bone loss and abnormal bone formation (Diboun et al., 2022)
COL9A2	collagen type IX alpha 2 chain	23	5 020 594	Related to cartilage (Klinger et al., 2017)
IGF2BP1	Insulin- like growth factor 2 mRNA binding protein 1	27	6 070 637–6 075 866	Related to the growth of bones (Wang et al., 2020)

Abbreviations: Chr = chromosomes.

growth curve in this model was well-matched with the phenotype of the actual chicken population, consistent with previous studies showing that the Logistic model is suitable for describing skeletal development in chickens (Wu et al., 2010; Zou et al., 2012). For the MeC trait, the Brody model appeared to be the most optimal growth curve model. Our data showed that MeL and MeC may exhibit different patterns of growth in chickens. Qiang et al. (2008) found that the Gompertz model was suitable for describing the growth and development of phalanx length in Zang chickens. Xie et al. (2020) found that the Gompertz and Bertalanffy models were optimal for representing the growth and development of feathers in yellow-feathered chickens at the embryonic and growing stages, respectively. Nguyen Hoang et al. (2021) used four growth curve models to fit the BW of Vietnamese Mia chickens and found that the Gompertz model was the most suitable model to describe the age–weight relationship. Based on these studies, we can conclude that different breeds and traits show unique growth trends, and thus, different models produce optimal growth curves in these animals. Additionally, sex also affects growth curve parameters. In this study, based on the optimal model, males had greater asymptotic maturity MeL and MeC values (MeL = 11.946, MeC = 4.632) than females (MeL = 9.496, meC = 3.959). Similar findings have been reported for BW and phalanx length in Zang chickens (Qiang et al., 2008). Moreover, a low maturity rate indicates delayed maturity, while a high value indicates accelerated maturity. In this study, the females reached maturity earlier than the males for both MeL (males = 0.277, females = 0.345) and MeC (males = 0.369, females = 0.541). Mata-Estrada et al. (2020) found that in the weight traits of Creole chickens from Mexico, the maturity rate of females was higher than that of males. This indicated that females generally reach maturity earlier than males, which is consistent with our findings. In summary, the data show that different species and traits exhibit different growth and development patterns. These growth curve parameters could guide daily feed management in chickens.

Single-trait and multi-trait genome-wide association study

So far, most studies on longitudinal traits (such as bone and BW) have employed observed phenotypic values at individual time points for GWAS rather than growth curve parameters. Actually, it seems more appropriate that the parameters of the growth curve are utilized as the input values of GWAS for longitudinal traits. This maybe lead to the identification of more significant genomic regions and SNPs associated with growth trajectories. In this study, we performed single-trait and multi-trait GWASs based on the growth curve parameters of the MeL and MeC traits in F_2 chickens. Accordingly, we identified a large number of genomic regions and genes involved in chicken bone growth and development. Single-trait and multi-trait GWASs have their respective advantages in the identification of QTLs responsible for traits of interest. Single-trait GWAS appears to be more powerful for identifying significant SNPs (Duan et al., 2021). In general, the QTLs that affect complex traits typically influence multiple traits simultaneously (Bolormaa et al., 2014). In this context, multi-trait GWAS can provide a higher statistical power than single-trait GWAS and identify pleiotropic loci (O'Reilly et al., 2012; Crispim et al., 2015). Therefore, a combination of both single-trait and multi-trait GWASs could significantly improve the identification of QTLs responsible for chicken bone traits.

In this study, we conducted both single-trait and multi-trait GWASs based on the growth curve parameters of the Logistic model for MeL and the Brody model for MeC traits. As a result, a total of 332 genes were annotated. In our previous study, Li et al. (2021b) employed single-time point and single-trait GWAS and found that the candidate genes affecting MeL and MeC develop-

Table 5
Novel quantitative trait loci (QTL) regions and candidate genes associated with the growth and development of chicken metatarsal length (MeL) and metatarsal circumference (MeC).

Chr	Position (kb)	Candidate genes
4	82 013–83 104	*RGS12*, *MSANTD1*, *HTT*, *GRK4*, *MFSD10*, *FAM193A*, *RNF4*, *CFAP99*, *ZFYVE28*, *MIR7467*, *MXD4*, *HAUS3*, *POLN*, *LOC107053322*, *LOC107056398*
5	55 379	*TA3*
6	17 813–18 953	*FBXL15*, *LOC101749795*, *LOC100858647*, *MSMB*, *ANTXRL*
10	6 187	*MAP2K5*
10	1 142–1 146	*TRNAQ-CUG*, *TRNAG-UCC*
10	19 757–19 761	*GLCE*
16	780	*LOC112533560*
19	867	*WBSCR27*
19	4 423–4 634	*SRRM3*, *MDH2*, *STYXL1*, *RFFL*
19	7 229	*LOC101747457*
22	3 696	*SNRNP200*
25	2 141	*LOC107051301*, *LOC107049929*

Abbreviations: Chr = Chromosomes.

ment were primarily located on GGA1 and 4. In contrast, our single-trait GWAS based on growth curve parameters not only yielded many previously identified candidate genes (including *RB1*, *RBPJ*, *PPARGC1A*, *FOXO1*, *SLIT2*, and *CPZ*) but also some novel genomic regions and candidate genes associated with skeletal development. In addition, the multi-trait GWAS based on growth curve parameters also found many pleiotropic loci and genes that had not been identified in previous studies. Our data revealed that multi-trait GWAS has more high statistical power in the identification of significant QTL. Moreover, in the present study, 295 and 241 genes were annotated via single-trait GWAS and multi-trait GWAS, respectively, and 204 of these genes overlapped (Supplementary Table S4). Hence, our data demonstrated that the combination of single-trait and multi-trait GWASs based on growth curve parameters can effectively identify more novel regions and candidate genes associated with metatarsal bone traits than single-time point and single-trait GWAS.

Novel candidate genes associated with the growth and development of chicken bones

We compared the physical locations of significant SNPs identified by GWAS with information from the Animal QTLdb. Accordingly, we discovered 12 novel QTLs related to the growth and development of chicken metatarsal bone traits, encompassing 35 candidate genes (Table 5 and Supplementary Table S4). Of these candidate genes, four genes (*RGS12*, *FAM193A*, *RNF4*, and *GLCE*) have been linked to skeletal traits in humans or mice (Table 4). Specifically, *RGS12* promotes osteoclastogenesis (Yuan et al., 2022), and *FAM193A* is associated with osteoporosis (Lee et al., 2019). Meanwhile, *RNF4* promotes osteoblast differentiation (Novak et al., 2022), and *GLCE* regulates a key cartilage signaling pathway (Chanalaris et al., 2019). So far, the remaining 31 genes have not been linked to bone traits in any other species. Nevertheless, our findings show that these genes may also act as candidate genes affecting bone growth and development, at least in chickens.

Conclusion

The growth curves fitted by the Logistic and Brody non-linear models were the most consistent with the MeL and MeC phenotypic records of our F_2 population, respectively. The combination of single-trait and multi-trait GWASs based on the growth curve parameters of the Logistic and Brody models revealed a large number of significant SNPs associated with metatarsal bone growth and development in chickens on a genome-wide scale. In particular, we identified 12 novel QTL regions located on GGA4, GGA5, GGA6, GGA10, GGA16, GGA19, GGA22, and GGA25, encompassing 35 candidate genes. Our findings provide a better understanding of the genetic architecture regulating bone growth and development traits in chickens and may contribute to selective breeding strategies in the future.

Supplementary material

Supplementary material to this article can be found online at https://doi.org/10.1016/j.animal.2024.101129.

Ethics approval

The animal study was reviewed and approved by the Laboratory Animal Management Committee of Northeast Agricultural University. This study was carried out following the Care and Use of Experimental Animals guidelines established by the Ministry of Science and Technology of the People's Republic of China (approval number 2006-398).

Data and model availability statement

None of the data were deposited in an official repository. Data may be available upon request by contacting the corresponding author.

Declaration of Generative AI and AI-assisted technologies in the writing process

During the preparation of this work the author(s) did not use any AI and AI-assisted technologies.

Author ORCIDs

Shouzhi Wang: https://orcid.org/0000-0002-0331-8626.
Mengdie Wang: https://orcid.org/0000-0002-7817-2764.
Jieyue Wang: https://orcid.org/0009-0004-3280-6196.
Meng Yuan: https://orcid.org/0000-0003-0964-2459.
Yudong Li: https://orcid.org/0000-0003-3436-3056.
Pingtao Luo: https://orcid.org/0009-0008-6690-4500.
Fan Xiao: https://orcid.org/0009-0007-9124-9643.
Hui Li: https://orcid.org/0000-0001-6282-5559.

CRediT authorship contribution statement

S.Z. Wang: Writing – review & editing, Methodology, Funding acquisition, Formal analysis, Conceptualization. **M.D. Wang:** Writing – review & editing, Writing – original draft, Methodology, Formal analysis, Data curation. **J.Y. Wang:** Writing – review & editing, Investigation, Data curation. **M. Yuan:** Writing – review & editing, Investigation, Data curation. **Y.D. Li:** Writing – review & editing, Data curation, Conceptualization. **P.T. Luo:** Investigation, Conceptualization. **F. Xiao:** Investigation, Conceptualization. **H. Li:** Writing – review & editing, Data curation, Conceptualization.

Declaration of interest

The authors declare that they have no conflict of interest.

Acknowledgements

The authors would like to acknowledge the members of the Key Laboratory of Chicken Genetics and Breeding at Northeast Agricultural University for managing the birds and collecting data.

Financial support statement

This work was supported by the Joint Guidance Project of Heilongjiang Natural Science Foundation (No. LH2021C036) and the earmarked fund for CARS-41.

References

Aggrey, S.E., 2002. Comparison of three nonlinear and spline regression models for describing chicken growth curves. Poultry Science 81, 1782–1788.
Aguado, E., Pascaretti-Grizon, F., Goyenvalle, E., Audran, M., Chappard, D., 2015. Bone mass and bone quality are altered by hypoactivity in the chicken. PloS One 10, e0116763.
Alam, I., Sun, Q., Koller, D.L., Liu, L., Liu, Y., Edenberg, H.J., Foroud, T., Turner, C.H., 2010. Genes influencing spinal bone mineral density in inbred F344, LEW, COP, and DA rats. Functional & Integrative Genomics 10, 63–72.
Aomatsu, E., Takahashi, N., Sawada, S., Okubo, N., Hasegawa, T., Taira, M., Miura, H., Ishisaki, A., Chosa, N., 2014. Novel SCRG1/BST1 axis regulates self-renewal, migration, and osteogenic differentiation potential in mesenchymal stem cells. Scientific Reports 4, 3652.
Ariza, Y., Murata, M., Ueda, Y., Yoshizawa, T., 2019. Bruton's tyrosine kinase (Btk) inhibitor tirabrutinib suppresses osteoclastic bone resorption. Bone Reports 10, 100201.
Assefa, F., Kim, J.A., Lim, J., Nam, S.H., Shin, H.I., Park, E.K., 2022. The Neuropeptide Spexin Promotes the osteoblast differentiation of MC3T3-E1 cells via the MEK/ERK pathway and bone regeneration in a mouse calvarial defect model. Tissue Engineering and Regenerative Medicine 19, 189–202.
Basal, O., Atay, T., Ciris, İ.M., Baykal, Y.B., 2018. Epidermal growth factor (EGF) promotes bone healing in surgically induced osteonecrosis of the femoral head (ONFH). Bosnian Journal of Basic Medical Sciences 18, 352–360.
Bolormaa, S., Pryce, J.E., Reverter, A., Zhang, Y., Barendse, W., Kemper, K., Tier, B., Savin, K., Hayes, B.J., Goddard, M.E., 2014. A multi-trait, meta-analysis for detecting pleiotropic polymorphisms for stature, fatness and reproduction in beef cattle. PLoS Genetics 10, e1004198.
Boonkum, W., Duangjinda, M., Kananit, S., Chankitisakul, V., Kenchaiwong, W., 2021. Genetic effect and growth curve parameter estimation under heat stress in slow-growing Thai native chickens. Veterinary Sciences 8, 297.
Born-Evers, G., Orr, A.L., Hulsey, E.Q., Squire, M.E., Hum, J.M., Plotkin, L., Sampson, C., Hommel, J., Lowery, J.W., 2023. Examining the role of hypothalamus-derived Neuromedin-U (NMU) in bone remodeling of rats. Life 13, 918.
Browning, B.L., Browning, S.R., 2009. A unified approach to genotype imputation and haplotype-phase inference for large data sets of trios and unrelated individuals. American Journal of Human Genetics 84, 210–223.
Cerani, A., Zhou, S., Forgetta, V., Morris, J.A., Trajanoska, K., Rivadeneira, F., Larsson, S.C., Michaëlsson, K., Richards, J.B., 2019. Genetic predisposition to increased serum calcium, bone mineral density, and fracture risk in individuals with normal calcium levels: mendelian randomisation study. British Medical Journal 366, l4410.
Chanalaris, A., Clarke, H., Guimond, S.E., Vincent, T.L., Turnbull, J.E., Troeberg, L., 2019. Heparan sulfate proteoglycan synthesis is dysregulated in human osteoarthritic cartilage. The American Journal of Pathology 189, 632–647.
Chang, M., He, L., Cai, L., 2018. An overview of genome-wide association studies. Methods in Molecular Biology 1754, 97–108.
Cheishvili, D., Parashar, S., Mahmood, N., Arakelian, A., Kremer, R., Goltzman, D., Szyf, M., Rabbani, S.A., 2018. Identification of an epigenetic signature of osteoporosis in blood DNA of postmenopausal women. Journal of Bone and Mineral Research 33, 1980–1989.
Cho, Y., Silverstein, R., Geisinger, M.T., Martinkovich, S., Corkill, H., Cunnick, J.M., Planey, S.L., Arnott, J.A., 2015. AFAP1 Is a novel downstream mediator of TGF-β1 for CCN2 induction in osteoblasts. PloS One 10, e0136712.
Choi, S.W., Shin, H.K., Yang-Yen, H.F., Lee, M.S., Lee, C.H., Park, S.J., Kim, K.J., Lee, K., Kim, S.H., 2014. Osteoclastogenic activity of translationally-controlled tumor protein (TCTP) with reciprocal repression of p21. FEBS Letters 588, 4026–4031.
Crispim, A.C., Kelly, M.J., Guimarães, S.E., Fonseca e Silva, F., Fortes, M.R., Wenceslau, R.R., Moore, S., 2015. Multi-trait gwas and new candidate genes annotation for growth curve parameters in brahman cattle. PloS One 10, e0139906.
Dale, M.D., Mortimer, E.M., Kolli, S., Achramowicz, E., Borchert, G., Juliano, S.A., Halkyard, S., Seitz, N., Gatto, C., Hester, P.Y., Rubin, D.A., 2015. Bone-remodeling transcript levels are independent of perching in end-of-lay white leghorn chickens. International Journal of Molecular Sciences 16, 2663–2677.
De Koning, D.J., Dominguez-Gasca, N., Fleming, R.H., Gill, A., Kurian, D., Law, A., McCormack, H.A., Morrice, D., Sanchez-Rodriguez, E., Rodriguez-Navarro, A.B., Preisinger, R., Schmutz, M., Šmídová, V., Turner, F., Wilson, P.W., Zhou, R., Dunn, I.C., 2020. An eQTL in the cystathionine beta synthase gene is linked to osteoporosis in laying hens. Genetics, Selection, Evolution: GSE 52, 13.
Diboun, I., Wani, S., Ralston, S.H., Albagha, O.M.E., 2022. Epigenetic DNA methylation signatures associated with the severity of paget's disease of bone. Frontiers in Cell and Developmental Biology 10, 903612.
Duan, X., An, B., Du, L., Chang, T., Liang, M., Yang, B.G., Xu, L., Zhang, L., Li, J., E, G., Gao, H., 2021. Genome-wide association analysis of growth curve parameters in chinese simmental beef cattle. Animals 11, 192.
Fleming, R.H., McCormack, H.A., McTeir, L., Whitehead, C.C., 2006. Relationships between genetic, environmental and nutritional factors influencing osteoporosis in laying hens. British Poultry Science 47, 742–755.
Gardinier, J.D., Chougule, A., Mendez, D., Daly-Seiler, C., Zhang, C., 2023. Periosteal bone formation varies with age in periostin null mice. Calcified Tissue International 112, 463–471.
Goto, N., Fujimoto, K., Fujii, S., Ida-Yonemochi, H., Ohshima, H., Kawamoto, T., Noshiro, M., Shukunami, C., Kozai, K., Kato, Y., 2016. Role of MSX1 in osteogenic differentiation of human dental pulp stem cells. Stem Cells International 2016, 8035759.
Guo, J., Qu, L., Dou, T.C., Shen, M.M., Hu, Y.P., Ma, M., Wang, K.H., 2020. Genome-wide association study provides insights into the genetic architecture of bone size and mass in chickens. Genome 63, 133–143.
Han, L., Wu, J., Wang, M., Zhang, Z., Hua, D., Lei, S., Mo, X., 2022. RNA modification-related genetic variants in genomic loci associated with bone mineral density and fracture. Genes 13, 1892.
Heisterkamp, S.H., Willigen, E.V., Diderichsen, P.M., Maringwa, J.T., 2017. Update of the nlme package to allow a fixed standard deviation of the residual error. R Journal 9, 239.
Hojjati, F., Ghavi Hossein-Zadeh, N., 2018. Comparison of non-linear growth models to describe the growth curve of Mehraban sheep. Journal of Applied Animal Research 46, 499–504.
Hoppman, N., McLenithan, J.C., McBride, D.J., Shen, H., Bruder, J., Bauer, R.L., Shaffer, J.R., Liu, J., Streeten, E.A., Shuldiner, A.R., Kammerer, C.M., Mitchell, B.D., 2010. A common variant in fibroblast growth factor binding protein 1 (FGFBP1) is associated with bone mineral density and influences gene expression in vitro. Bone 47, 272–280.
Huang, X., Su, X., Ma, Q., Xie, Y., Guo, Q., Liao, L., Zou, J., 2023. FoxO1 Agonists promote bone regeneration in periodontitis by protecting the osteogenesis of periodontal ligament stem cells. Stem Cells and Development 32, 491–503.
Huang, Y., Xiao, L., Zhang, Z., Zhang, R., Wang, Z., Huang, C., Huang, R., Luan, Y., Fan, T., Wang, J., Shen, C., Zhang, S., Wang, X., Randall, J., Zheng, B., Wu, J., Zhang, Q., Xia, G., Xu, C., Chen, M., Zhang, L., Jiang, W., Gao, L., Chen, Z., Leslie, C., Grauke, L., Huang, J., 2019. The genomes of pecan and Chinese hickory provide insights into Carya evolution and nut nutrition. GigaScience 8, giz036.
Jansen, S., Baulain, U., Habig, C., Weigend, A., Halle, I., Scholz, A.M., Simianer, H., Sharifi, A.R., Weigend, S., 2020. Relationship between bone stability and egg production in genetically divergent chicken layer lines. Animals 10, 850.
Johnsson, M., Wall, H., Lopes Pinto, F.A., Fleming, R.H., McCormack, H.A., Benavides-Reyes, C., Dominguez-Gasca, N., Sanchez-Rodriguez, E., Dunn, I.C., Rodriguez-Navarro, A.B., Kindmark, A., de Koning, D.J., 2023. Genetics of tibia bone properties of crossbred commercial laying hens in different housing systems. G3-Genes Genomes. Genetics 13, jkac302.
Kellogg, E.C., Thrasher, A., Yoshinaga-Itano, C., 2014. Early predictors of autism in young children who are deaf or hard of hearing: three longitudinal case studies. Seminars in Speech and Language 35, 276–287.
Kim, H., Takegahara, N., Walsh, M.C., Ueda, J., Fujihara, Y., Ikawa, M., Choi, Y., 2020. Protocadherin-7 contributes to maintenance of bone homeostasis through regulation of osteoclast multinucleation. Bioscience, Biotechnology, and Biochemistry Reports 53, 472–477.
Klinger, P., Lukassen, S., Ferrazzi, F., Ekici, A.B., Hotfiel, T., Swoboda, B., Aigner, T., Gelse, K., 2017. PEDF is associated with the termination of chondrocyte phenotype and catabolism of cartilage tissue. BioMed Research International 2017, 7183516.
Knöpfel, T., Pastor-Arroyo, E.M., Schnitzbauer, U., Kratschmar, D.V., Odermatt, A., Pellegrini, G., Hernando, N., Wagner, C.A., 2017. The intestinal phosphate transporter NaPi-IIb (Slc34a2) is required to protect bone during dietary phosphate restriction. Scientific Reports 7, 11018.
Kwon, E.K., Louie, K., Kulkarni, A., Yatabe, M., Ruellas, A.C.O., Snider, T.N., Mochida, Y., Cevidanes, L.H.S., Mishina, Y., Zhang, H., 2018. The role of Ellis-Van Creveld 2 (EVC2) in mice during cranial bone development. Anatomical Record 301, 46–55.
Lee, L., Atkinson, D., Hirst, A.G., Cornell, S.J., 2020. A new framework for growth curve fitting based on the von Bertalanffy growth function. Scientific Reports 10, 7953.
Lee, S.A., Choi, J.Y., Shin, C.S., Hong, Y.C., Chung, H., Kang, D., 2006. SULT1E1 genetic polymorphisms modified the association between phytoestrogen consumption and bone mineral density in healthy Korean women. Calcified Tissue International 79, 152–159.
Lee, K.H., Kim, S.H., Kim, C.H., Min, B.J., Kim, G.J., Lim, Y., Kim, H.S., Ahn, K.M., Kim, J. H., 2019. Identifying genetic variants underlying medication-induced

osteonecrosis of the jaw in cancer and osteoporosis: a case control study. Journal of Translational Medicine 17, 381.
Leng, L., Wang, S., Li, Z., Wang, Q., Li, H., 2009. A polymorphism in the 3'-flanking region of insulin-like growth factor binding protein 2 gene associated with abdominal fat in chickens. Poultry Science 88, 938–942.
Li, H., Durbin, R., 2009. Fast and accurate short read alignment with Burrows-Wheeler transform. Bioinformatics (Oxford, England) 25, 1754–1760.
Li, H., Handsaker, B., Wysoker, A., Fennell, T., Ruan, J., Homer, N., Marth, G., Abecasis, G., Durbin, R., 1000 genome project data processing subgroup., 2009. The sequence alignment/map format and SAMtools. Bioinformatics (Oxford, England) 25, pp. 2078–2079.
Li, Y.D., Liu, X., Li, Z.W., Wang, W.J., Li, Y.M., Cao, Z.P., Luan, P., Xiao, F., Gao, H.H., Guo, H.S., Wang, N., Li, H., Wang, S.Z., 2021b. A combination of genome-wide association study and selection signature analysis dissects the genetic architecture underlying bone traits in chickens. Animal 15, 100322.
Li, H., Lu, A., Gao, X., Tang, Y., Ravuri, S., Wang, B., Huard, J., 2021a. Improved bone quality and bone healing of dystrophic mice by parabiosis. Metabolites 11, 247.
Li, S., Miller, C.H., Giannopoulou, E., Hu, X., Ivashkiv, L.B., Zhao, B., 2014. RBP-J imposes a requirement for ITAM-mediated costimulation of osteoclastogenesis. The Journal of Clinical Investigation 124, 5057–5073.
Li, Y., Yang, S., Yang, S., 2022. Rb1 negatively regulates bone formation and remodeling through inhibiting transcriptional regulation of YAP in Glut1 and OPG expression and glucose metabolism in male mice. Molecular Metabolism 66, 101630.
Ma, Z., He, S., Wang, X., Sun, J., Zhang, Y., Zhang, G., Wu, L., Li, Z., Liu, Z., Sun, G., Yan, Y., Jia, Y., Yang, J., Pan, Z., Gu, Q., Li, X., Sun, Z., Dai, P., Liu, Z., Gong, W., Wu, J., Wang, M., Liu, H., Feng, K., Ke, H., Wang, J., Lan, H., Wang, G., Peng, J., Wang, N., Wang, L., Pang, B., Peng, Z., Li, R., Tian, S., Du, X., 2018. Resequencing a core collection of upland cotton identifies genomic variation and loci influencing fiber quality and yield. Nature Genetics 50, 803–813.
Ma, J.J., Ying, J., Wang, J.Y., Xu, T.T., Xia, H.T., Jin, H.T., Xiao, L.W., Shang, W.J., Wang, W.Q., Feng, J.Y., 2022. CD38 Drives progress of osteoarthritis by affecting cartilage homeostasis. Orthopaedic Surgery 14, 946–954.
Mata-Estrada, A., González-Cerón, F., Pro-Martínez, A., Torres-Hernández, G., Bautista-Ortega, J., Becerril-Pérez, C.M., Vargas-Galicia, A.J., Sosa-Montes, E., 2020. Comparison of four nonlinear growth models in Creole chickens of Mexico. Poultry Science 99, 1995–2000.
Mesner, L.D., Calabrese, G.M., Al-Barghouthi, B., Gatti, D.M., Sundberg, J.P., Churchill, G.A., Godfrey, D.A., Ackert-Bicknell, C.L., Farber, C.R., 2019. Mouse genome-wide association and systems genetics identifies Lhfp as a regulator of bone mass. PLoS Genetics 15, e1008123.
Miao, J., Wang, X., Bao, J., Jin, S., Chang, T., Xia, J., Yang, L., Zhu, B., Xu, L., Zhang, L., Gao, X., Chen, Y., Li, J., Gao, H., 2018. Multimarker and rare variants genomewide association studies for bone weight in Simmental cattle. Journal of Animal Breeding and Genetics 135, 159–169.
Mignon-Grasteau, S., Beaumont, C., Le Bihan-Duval, E., Poivey, J.P., De Rochambeau, H., Ricard, F.H., 1999. Genetic parameters of growth curve parameters in male and female chickens. British Poultry Science 40, 44–51.
Mokhtari, M.S., Borzi, N.K., Fozi, M.A., Behzadi, M.R.B., 2019. Evaluation of non-linear models for genetic parameters estimation of growth curve traits in Kermani sheep. Tropical Animal Health and Production 51, 2203–2212.
Murakami, K., Zhifeng, H., Suzuki, T., Kobayashi, Y., Nakamura, Y., 2019. The Shisa3 knockout mouse exhibits normal bone phenotype. Journal of Bone and Mineral Metabolism 37, 967–975.
Narinç, D., Öksüz Narinç, N., Aygün, A., 2017. Growth curve analyses in poultry science. World's Poultry Science Journal 73, 395–408.
National Research Council, 1994. Nutrient requirements of poultry (Ninth Revised Edition). The National Academies Press, Washington, DC.
Nguyen Hoang, T., Do, H.T.T., Bui, D.H., Pham, D.K., Hoang, T.A., Do, D.N., 2021. Evaluation of non-linear growth curve models in the Vietnamese indigenous Mia chicken. Animal Science Journal 92, e13483.
Nguyen, T.H., Nguyen, C.X., Luu, M.Q., Nguyen, A.T., Bui, D.H., Pham, D.K., Do, D.N., 2021. Mathematical models to describe the growth curves of Vietnamese Ri chicken. Brazilian Journal of Biology 83, e249756.
Ning, C., Wang, D., Zheng, X., Zhang, Q., Zhang, S., Mrode, R., Liu, J.F., 2018. Eigen decomposition expedites longitudinal genome-wide association studies for milk production traits in Chinese Holstein. Genetics, Selection, Evolution: GSE 50, 12.
Niu, Q., Zhang, T., Xu, L., Wang, T., Wang, Z., Zhu, B., Gao, X., Chen, Y., Zhang, L., Gao, H., Li, J., Xu, L., 2021. Identification of candidate variants associated with bone weight using whole genome sequence in beef cattle. Frontiers in Genetics 12, 750746.
Nordberg, R.C., Wang, H., Wu, Q., Loboa, E.G., 2018. Corin is a key regulator of endochondral ossification and bone development via modulation of vascular endothelial growth factor a expression. Journal of Tissue Engineering and Regenerative Medicine 12, 2277–2286.
Novak, R., Ahmad, Y.A., Timaner, M., Bitman-Lotan, E., Oknin-Vaisman, A., Horwitz, R., Hartmann, O., Reissland, M., Buck, V., Rosenfeldt, M., Nikomarov, D., Diefenbacher, M.E., Shaked, Y., Orian, A., 2022. RNF4∼RGMb∼BMP6 axis required for osteogenic differentiation and cancer cell survival. Cell Death & Disease 13, 820.
Oh, M.R., Lee, K.J., Huang, M., Kim, J.O., Kim, D.H., Cho, C.H., Lee, E.H., 2017. STIM2 regulates both intracellular Ca2+ distribution and Ca2+ movement in skeletal myotubes. Scientific Reports 7, 17936.
Oliveira, H.R., Lourenco, D.A.L., Masuda, Y., Misztal, I., Tsuruta, S., Jamrozik, J., Brito, L.F., Silva, F.F., Cant, J.P., Schenkel, F.S., 2019. Single-step genome-wide association for longitudinal traits of Canadian Ayrshire, Holstein, and Jersey dairy cattle. Journal of Dairy Science 102, 9995–10011.
O'Reilly, P.F., Hoggart, C.J., Pomyen, Y., Calboli, F.C., Elliott, P., Jarvelin, M.R., Coin, L.J., 2012. MultiPhen: joint model of multiple phenotypes can increase discovery in GWAS. PloS One 7, e34861.
Park, S.J., Lee, J.Y., Lee, S.H., Koh, J.M., Kim, B.J., 2019. SLIT2 inhibits osteoclastogenesis and bone resorption by suppression of Cdc42 activity. Biochemical and Biophysical Research Communications 514, 868–874.
Purcell, S., Neale, B., Todd-Brown, K., Thomas, L., Ferreira, M.A., Bender, D., Maller, J., Sklar, P., de Bakker, P.I., Daly, M.J., Sham, P.C., 2007. PLINK: a tool set for whole-genome association and population-based linkage analyses. American Journal of Human Genetics 81, 559–575.
Qiang, B.Y.Z., Zhai, M.X., Xie, Z., Li, Q.F., 2008. Gompertz growth curves of body weight and phalanx length, and regression analysis in Zang chicken. Journal of Nanjing Agricultural University 02, 86–90 (in Chinese).
Seifi Moroudi, R., Ansari Mahyari, S., Vaez Torshizi, R., Lanjanian, H., Masoudi-Nejad, A., 2021. Identification of new genes and quantitative trait locis associated with growth curve parameters in F2 chicken population using genome-wide association study. Animal Genetics 52, 171–184.
Snelling, S., Sinsheimer, J.S., Carr, A., Loughlin, J., 2007. Genetic association analysis of LRCH1 as an osteoarthritis susceptibility locus. Rheumatology (Oxford, England) 46, 250–252.
Soares, A.C.C., Guimarães, S.E.F., Kelly, M.J., Fortes, M.R.S., E Silva, F.F., Verardo, L.L., Mota, R., Moore, S., 2017. Multiple-trait genomewide mapping and gene network analysis for scrotal circumference growth curves in Brahman cattle. Journal of Animal Science 95, 3331–3345.
Symoens, S., Barnes, A.M., Gistelinck, C., Malfait, F., Guillemyn, B., Steyaert, W., Syx, D., D'hondt, S., Biervliet, M., De Backer, J., Witten, E.P., Leikin, S., Makareeva, E., Gillessen-Kaesbach, G., Huysseune, A., Vleminckx, K., Willaert, A., De Paepe, A., Marini, J.C., Coucke, P.J., 2015. Genetic defects in TAPT1 disrupt ciliogenesis and cause a complex lethal osteochondrodysplasia. American Journal of Human Genetics 97, 521–534.
Tang, C.Y., Wang, H., Zhang, Y., Wang, Z., Zhu, G., McVicar, A., Li, Y.P., Chen, W., 2022. GPR125 positively regulates osteoclastogenesis potentially through AKT-NF-κB and MAPK signaling pathways. International Journal of Biological Sciences 18, 2392–2405.
Waldmann, L., Leyhr, J., Zhang, H., Öhman-Mägi, C., Allalou, A., Haitina, T., 2021. The broad role of Nkx3.2 in the development of the zebrafish axial skeleton. PloS One 16, e0255953.
Wang, Y., Bu, L., Cao, X., Qu, H., Zhang, C., Ren, J., Huang, Z., Zhao, Y., Luo, C., Hu, X., Shu, D., Li, N., 2020. Genetic dissection of growth traits in a unique chicken advanced intercross line. Frontiers in Genetics 11, 894.
Wang, K., Li, M., Hakonarson, H., 2010. ANNOVAR: functional annotation of genetic variants from high-throughput sequencing data. Nucleic Acids Research 38, e164.
Wang, S., Wang, Y., Li, Y., Xiao, F., Guo, H., Gao, H., Wang, N., Zhang, H., Li, H., 2022. Genome-wide association study and selective sweep analysis reveal the genetic architecture of body weights in a chicken F2 resource population. Frontiers in Veterinary Science 9, 875454.
Wu, W.G., Cao, X., Xu, M.J., 2010. A study on fitting the growth curve of Hunan yellow hens. Animal Husbandry and Feed Science 31, 9–11 (in Chinese).
Xie, W.Y., Pan, N.X., Zeng, H.R., Yan, H.C., Wang, X.Q., Gao, C.Q., 2020. Comparison of nonlinear models to describe the feather growth and development curve in yellow-feathered chickens. Animal 14, 1005–1013.
Yang, W., Xia, Y., Qian, X., Wang, M., Zhang, X., Li, Y., Li, L., 2019. Co-expression network analysis identified key genes in association with mesenchymal stem cell osteogenic differentiation. Cell and Tissue Research 378, 513–529.
Yin, L., Zhang, H., Tang, Z., Xu, J., Yin, D., Zhang, Z., Yuan, X., Zhu, M., Zhao, S., Li, X., Liu, X., 2021. rMVP: a memory-efficient, visualization-enhanced, and parallel-accelerated tool for genome-wide association study. Genomics Proteomics Bioinformatics 19, 619–628.
Yu, B., Huo, L., Liu, Y., Deng, P., Szymanski, J., Li, J., Luo, X., Hong, C., Lin, J., Wang, C.Y., 2018. PGC-1α controls skeletal stem cell fate and bone-fat balance in osteoporosis and skeletal aging by inducing TAZ. Cell Stem Cell 23, 193–209.e5.
Yuan, G., Fu, C., Yang, S.T., Yuh, D.Y., Hajishengallis, G., Yang, S., 2022. RGS12 drives macrophage activation and osteoclastogenesis in periodontitis. Journal of Dental Research 101, 448–457.
Zhang, H., Zhang, Y.D., Wang, S.Z., Liu, X.F., Zhang, Q., Tang, Z.Q., Li, H., 2010. Detection and fine mapping of quantitative trait loci for bone traits on chicken chromosome one. Journal of Animal Breeding and Genetics 127, 462–468.
Zhang, H., Liu, S.H., Zhang, Q., Zhang, Y.D., Wang, S.Z., Wang, Q.G., Wang, Y.X., Tang, Z.Q., Li, H., 2011. Fine-mapping of quantitative trait loci for body weight and bone traits and positional cloning of the RB1 gene in chicken. Journal of Animal Breeding and Genetics 128, 366–375.
Zhang, H., Shen, L.Y., Xu, Z.C., Kramer, L.M., Yu, J.Q., Zhang, X.Y., Na, W., Yang, L.L., Cao, Z.P., Luan, P., Reecy, J.M., Li, H., 2020. Haplotype-based genome-wide association studies for carcass and growth traits in chicken. Poultry Science 99, 2349–2361.
Zhou, X., Stephens, M., 2012. Genome-wide efficient mixed-model analysis for association studies. Nature Genetics 44, 821–824.
Zhu, W., Yang, X., Liu, S., Wang, M., Ye, S., Luo, H., Cui, S., 2020. The involvement of cytokine-like 1 (Cytl1) in chondrogenesis and cartilage metabolism. Biochemical and Biophysical Research Communications 529, 608–614.
Zou, J.M., Song, C., Shan, J.Y., Song, W.T., Shu, J.T., 2012. Fitting of body weight and tibial length growth curve of Qingyuan Ma chicken. Jiangsu Agricultural Sciences 40, 213–215 (in Chinese).